Published in final edited form as:
Cell Stem Cell. 2013 September 5; 13(3): . doi:10.1016/j.stem.2013.06.018.

Architectural Niche Organization by LHX2 Is Linked to Hair Follicle Stem Cell Function

Alicia R. Folgueras[1], **Xingyi Guo**[2], **H. Amalia Pasolli**[1], **Nicole Stokes**[1], **Lisa Polak**[1], **Deyou Zheng**[2,3,4], and **Elaine Fuchs**[1,*]

[1]Howard Hughes Medical Institute, Laboratory of Mammalian Cell Biology and Development, The Rockefeller University, New York, NY 10065, USA

[2]Department of Neurology, Albert Einstein College of Medicine, Bronx, NY 10461, USA

[3]Department of Genetics, Albert Einstein College of Medicine, Bronx, NY 10461, USA

[4]Department of Neuroscience, Albert Einstein College of Medicine, Bronx, NY 10461, USA

SUMMARY

In adult skin, self-renewing, undifferentiated hair follicle stem cells (HF-SCs) reside within a specialized niche, where they spend prolonged times as a single layer of polarized, quiescent epithelial cells. When sufficient activating signals accumulate, HF-SCs become mobilized to fuel tissue regeneration and hair growth. Here, we show that architectural organization of the HF-SC niche by transcription factor LHX2 plays a critical role in HF-SC behavior. Using genome-wide chromatin and transcriptional profiling of HF-SCs in vivo, we show that LHX2 directly transactivates genes that orchestrate cytoskeletal dynamics and adhesion. Conditional ablation of LHX2 results in gross cellular disorganization and HF-SC polarization within the niche. LHX2 loss leads to a failure to maintain HF-SC quiescence and hair anchoring, as well as progressive transformation of the niche into a sebaceous gland. These findings suggest that niche organization underlies the requirement for LHX2 in hair follicle structure and function.

INTRODUCTION

Adult stem cells (SCs) reside in specialized niches, where they often exist in a quiescent state until self-renewal and differentiation programs are activated to guarantee tissue homeostasis or wound-repair (Hsu and Fuchs, 2012). In the hair follicle (HF), multipotent SCs have been identified in the outermost layer of an anatomically distinct region called the bulge, situated just below the sebaceous glands (SGs) and at the base of resting follicles (Cotsarelis et al., 1990; Tumbar et al., 2004).

HF-SCs first appear late in embryogenesis, during which they are typified by their slow-cycling nature and expression of transcription factors TCF3, TCF4, SOX9, NFATc1, and LHX2, all of which are essential for HF morphogenesis (Blanpain and Fuchs, 2009). Lineage tracing shows that once HF-SCs emerge in embryogenesis, they replace existing

*Correspondence: fuchslb@rockefeller.edu.

ACCESSION NUMBERS

ChIP-seq data have been deposited in the Gene Expression Omnibus data-base under the accession number GSE48068.

SUPPLEMENTAL INFORMATION

Supplemental Information includes Supplemental Experimental Procedures, seven figures, and one table and can be found with this article online at http://dx.doi.org/10.1016/j.stem.2013.06.018.

cells within developing HFs and drive SG morphogenesis (Nowak et al., 2008). During normal homeostasis in the adult, HF-SCs function in the regenerative phases of hair cycling, but upon injury, they can repair epidermis and SGs (Blanpain et al., 2004; Brownell et al., 2011; Horsley et al., 2006; Ito et al., 2005).

At the start of the growth phase (anagen), cells at the base of the bulge (hair germ, HG), which are initially similar to bulge HF-SCs in gene expression (Greco et al., 2009), become proliferative, grow downward, and engulf the transient mesenchymal niche component (dermal papilla, DP) as they transition to committed, so-called transit-amplifying matrix cells (TACs). TACs continue to proliferate in the hair bulb at the bottom of the mature HF and terminally differentiate to form the hair and its channel (inner root sheath, IRS).

During early anagen, as the HF is regenerating and the DP is pushed downward away from the niche, HF-SCs from the bulge form a trail of cells along the outer root sheath (ORS) of the follicle. Upper ORS cells divide only a few times before returning to quiescence; these cells retain their stemness and form the new bulge for the next hair cycle (Hsu et al., 2011). When the destructive phase (catagen) ensues and TACs apoptose, some lower ORS cells are spared, short-circuiting the matrix. They wind up at catagen's end as an inner layer of terminally differentiated bulge cells that anchor the hair and transmit inhibitory BMP6 and FGF18 signals to HF-SCs (Hsu et al., 2011). During the resting phase (telogen), HF-SCs and HG remain quiescent until sufficient activating cues accumulate in the niche to launch a new hair cycle.

The mechanisms underlying the intricate balance between long-term self-renewal of HF-SCs and their commitment into differentiated lineages are still poorly understood. In addition to the inner bulge layer, the niche provides a rich milieu of activating and inhibitory signals to control SC dynamics (Brownell et al., 2011; Festa et al., 2011; Greco et al., 2009; Plikus et al., 2008). Wnts seem to be particularly critical at anagen onset. Additionally, later in the lineage, elevated Wnt signaling in TACs drives their differentiation into hair cells (DasGupta and Fuchs, 1999).

Although these studies begin to suggest how stemness is influenced by external signaling pathways, less is known about the impact of cytoarchitecture on HF-SC behavior. The factors necessary for generating the niche are likely to come from the HF-SCs themselves, because purified bulge HF-SCs engrafted to *Nude* mice can recruit surrounding dermal components to recreate a seemingly functional, cycling HF replete with a bulge (Blanpain et al., 2004). Additionally at the molecular level, bulge HF-SCs are enriched in transcripts encoding specific cell-cell, cytoskeletal, and cell-extracellular matrix (ECM) adhesion proteins. However, a largely unexplored issue for HF-SCs in particular and SCs in general is whether cellular organization is an essential feature within the niche, and if so, how it is transcriptionally governed.

Our interest in these issues began with a continued focus on Lim-homeodomain transcription factor LHX2. *Lhx2*-null mice die around embryonic day 16.5 (E16.5) due to severe anemia (Porter et al., 1997). However, LHX2 is expressed in the early hair placode, and when engrafted, *Lhx2*-null skin shows a sparser hair coat accompanied by an apparent failure of HFs to properly maintain a resting state (Rhee et al., 2006). In addition, mice heterozygous for the mutant *Lhx2* allele heal wounds more slowly (Mardaryev et al., 2011). Hence, despite a recent study claiming that LHX2 is neither expressed nor functional in HF-SCs (Törnqvist et al., 2010), the effects of LHX2 loss on hair cycling and wound repair are suggestive, albeit as yet untested, that LHX2 controls some aspect of HF-SC behavior (Mardaryev et al., 2011; Rhee et al., 2006).

Increasing evidence suggests that LHX2's role may also extend to many other SCs, even those in more ancient eukaryotes such as *C. elegans* (Bertrand and Hobert, 2009; Hägglund et al., 2011; Kitajima et al., 2011; Mangale et al., 2008; Mardaryev et al., 2011; Subramanian et al., 2011; Xu et al., 2007). Again, however, how LHX2 functions in any SC remains poorly understood. Thus far, very few LHX2 target genes have been identified. Only one report of chromatin-wide mapping of LHX2 binding sites has been performed, and this was on primary keratinocytes from embryonic back skin (Mardaryev et al., 2011). Given accumulating evidence that cell type and stage specificity dictate the binding of transcription factors and chromatin modifiers (Mullen et al., 2011; Trompouki et al., 2011), it seemed probable that identifying LHX2's targets and elucidating the function(s) of LHX2 on SC biology would be predicated on studying LHX2 in SCs. Our findings reported here bear out this premise.

In this study, we use HFs as our model system to explore whether and how LHX2 functions in adult SC biology and normal homeostasis. We first perform in vivo anti-LHX2 chromatin immunoprecipitation and deep sequencing (ChIP-seq) on purified HF-SCs taken directly from their native niche. Second, we perform skin-specific conditional ablation of *Lhx2* in mice and couple our newfound knowledge of LHX2-bound genes in HF-SCs with transcriptional profiling of messenger RNAs (mRNAs) from wild-type and *K14-Cre*/*Lhx2*$^{fl/fl}$ conditional knockout (*Lhx2*-cKO) HF-SC-enriched populations. Our studies show that LHX2 regulates a significant number of HF-SC signature genes and cytoskeletal and adhesion molecules within the niche. Delving into the physiological relevance of these findings, we unearth a surprising reason for why LHX2 loss leads to baldness. Rather than exhausting HF-SC proliferative activity or blocking Wnt signaling at the niche base, LHX2 deficiency profoundly perturbs HF-SC polarization and niche architecture. Without LHX2, the niche can no longer anchor its hair and maintain the proper behavior of its SCs.

RESULTS

Direct LHX2 Target Genes in HF-SCs are Dramatically Different from Those Seen in Embryonic Skin Keratinocytes

To conditionally ablate *Lhx2* in skin epithelium, we used the *Krt14* promoter to drive Cre-recombinase, which is robustly active by E15.5, when most hair buds begin to develop (Vasioukhin et al., 1999). *Lhx2*-cKO mice were viable and appeared in the expected Mendelian ratios. We monitored LHX2 with a newly generated antibody and *Lhx2* promoter activity by using mice transgenic for *Lhx2-EGFP* (Gene Expression Nervous System Atlas).

During embryogenesis, LHX2 was first detected in the nuclei of cells at the leading front of hair buds (Figure 1A). As development progressed, immunolabeling and *Lhx2-EGFP* expression waned in the matrix and became prominent in emerging HF-SCs (Figures 1B-1D). HF-SC expression of LHX2 persisted throughout adulthood and did not waver with hair cycle (Figures 1C-1E). Labeling was specific, given that it was absent in *Lhx2*-cKO skin. Together, these findings underscored the efficacy of both our gene targeting and LHX2 antibody and confirmed LHX2's presence in HF-SCs, as suggested in two prior reports (Mardaryev et al., 2011; Rhee et al., 2006), but in contrast to a third (Törnqvist et al., 2010).

HF-SCs are among the few SCs that can be purified in sufficient quantities for conducting ChIP-seq in vivo. This enabled us to directly address the extent to which LHX2 target genes previously reported for embryonic skin keratinocytes (Mardaryev et al., 2011) have relevance to adult bulge HF-SCs. The study took on all the more importance given that LHX2's expression in embryonic skin is diverse and that the majority of cells within this tissue do not express LHX2 at all.

ChIP-seq was performed in triplicate on $\alpha6^{hi}/CD34^{+}$ cells, which are enriched for HF-SCs, isolated by fluorescence-activated cell sorting (FACS) from second telogen HFs (Figure S1 available online). After aligning ChIP-seq reads to the mouse genome, we called a total of 2,368 LHX2 peaks with strict criteria. Importantly, a classic LHX2 binding motif was identified within 79% of LHX2 peaks, underscoring the reliability of these calls (Figure 1F). Moreover, LHX2 peaks were enriched in promoters (±2 kb of transcription start sites) and "enhancers" (−50 kb upstream to +5 kb downstream of gene body) of annotated mouse RefSeq genes (Figure 1G). Based on these criteria, 1,512 of the 2,368 LHX2 peaks associated with genes and 1,115 different genes showed direct LHX2 binding in either their promoters or enhancers.

Less than 4% of the LHX2 targets from our enriched population of adult HF-SCs had been reported previously as LHX2 targets of embryonic skin (Mardaryev et al., 2011) (Figure 1H). Notably, >20% (three times higher than expected by chance) of our ChIP-seq targets were also enriched in HF-SCs compared to their progeny (Lien et al., 2011). By contrast, only 7% of LHX2 targets found in embryonic skin (Mardaryev et al., 2011) were part of the HF-SC signature (Figure 1H). Although variations in approach and analysis can lead to differences, our findings also underscored the importance of cell type and context in identifying target genes by chromatin mapping.

HFs Lacking LHX2 Are Specifically Defective in Establishing and Maintaining SCs

The preponderance of HF-SC signature genes that bound LHX2 coupled with LHX2's clear expression in adult HF-SCs suggested that this transcription factor may play a key role in stemness. To pursue this possibility, we focused on postnatal development, in which the consequences of LHX2-deficiency had not been explored.

Interestingly, signs of HF-SC perturbations were already apparent at birth (P0), as evidenced by immunolabeling for an early HF-SC marker, transcription factor SOX9. As shown in Figure 2A, the location of SOX9 within the ORS in *Lhx2*-cKO HFs was distinctly lower than in wild-type (WT) HFs. Immunofluorescence and FACS (Blanpain et al., 2004) further revealed that other markers of HF-SCs, NFATc1 and CD34, were also diminished in *Lhx2*-cKO HFs (Figures 2B-2D).

Several additional defects were noted within developing *Lhx2*-cKO HF-SCs. In contrast to WT (Nowak et al., 2008), the developing bulge region of P6 *Lhx2*-cKO HFs showed continued proliferation, and yet hair bulbs were small (Figures S2A and S2B). A priori, this feature could reflect either an intrinsic defect in matrix cell behavior, as suggested previously (Törnqvist et al., 2010), or alternatively, a failure of HF-SCs to adequately fuel the pool of TACs. To distinguish between these possibilities, we conducted pulse-chase experiments with nucleotide analogs. Although the *Lhx2*-cKO matrix had fewer total cells and fewer EdU^{+} cells after 4 hr, the overall percentage of labeled cells in this compartment was comparable to WT, as was the percentage of EdU^{+} matrix cells that progressed into terminal differentiated lineages by 14 hr of labeling (Figure S2B).

Based upon these criteria, although the rate of flux differed, *Lhx2*-cKO matrix TACs behaved normally in cycling and progression through their lineage-differentiation routes. This was further evidenced by the fact that although *Lhx2*-cKO HFs exhibited a slightly prolonged first anagen, they did enter catagen, and they progressed into telogen (Figures S2C and S2D).

Taken together, these findings continued to point to a defect in HF-SCs (Nowak et al., 2008). Moreover, as *Lhx2*-cKO HFs matured and cycled, the location of the bulge niche

remained low, and alterations in HF-SC markers did not resolve. *Lhx2*-cKO mice became bald over time (Figure 2E).

Lhx2-cKO HFs: Early Defects in SCs but Normal Mechanics of Lineage Progression

Our prior studies with engrafted skins from P0 *Lhx2*-null mice suggested that HFs lacking LHX2 were not slow cycling (Rhee et al., 2006). Our *Lhx2*-cKO mice now allowed us to extend these findings to the natural skin context. In WT HFs, HF-SCs within the bulge proliferate in early anagen, whereas those in the upper ORS trail extending down from the bulge remain proliferative until mid-late anagen (Hsu et al., 2011). A series of short bromodeoxyuridine (BrdU) pulses during the first postnatal anagen from P23→P25 (early-mid anagen) uniformly labeled slow-cycling HF-SCs and fast-cycling TACs in the ORS (Figure 3A). Following a 50 day chase, $BrdU^+$, label-retaining cells were diminished by >10× in *Lhx2*-cKO HFs. By recapitulating the loss of label retention in otherwise unperturbed *Lhx2*-cKO HF-SCs, these data show that the feature is attributable to an intrinsic defect of HF-SCs and not dependent upon a wound-induced response.

To evaluate the consequences of increased SC activity over multiple hair cycles, we next shaved hair coats during the second telogen phase, and then monitored hair regrowth. In contrast to WT, *Lhx2*-cKO mice regrew their hair coat within a week after shaving (Figure 3B). Histological analyses confirmed that at P49, *Lhx2*-cKO HFs were in full anagen (Figure 3C). A 24 hr BrdU pulse revealed that even at P45, when WT HFs had just entered their second telogen, *Lhx2*-cKO HFs were already showing proliferative signs of entering their third anagen (Figure 3D).

Interestingly, even though older *Lhx2*-cKO HFs continued to cycle and did so much more rapidly than WT HFs, they still entered a brief telogen phase, as evidenced by lack of BrdU incorporation in the bulge (Figure 3D). This was further substantiated by modest transcriptional changes in cyclins, known to be upregulated in HF-SCs at anagen onset (Lien et al., 2011) (Figure 3F). Moreover, despite the short (1–2 day) telogen phase, *Lhx2*-cKO HFs still maintained a two-tier structure of bulge and HG (Greco et al., 2009; Hsu et al., 2011), and the sequential activation of these two units appeared to be intact (see Figure 3D). This was confirmed by mating *Lhx2*-cKO mice on the background of $Axin2^{LacZ/+}$, a powerful Wnt-responsive gene (Figure 3E). The induction of $Axin2^{LacZ/+}$ activity within the HG at telogen→anagen transition correlated with the nuclear β-catenin and proliferation known to occur in WT HG cells at this time (Greco et al., 2009). Thus, although precocious, the mechanism of SC activation and lineage progression appeared to be operative in the absence of LHX2.

Loss of LHX2: More Than Simply Precocious Activation of the Hair Cycle

Our data thus far suggested that LHX2-deficient HF-SCs might be expended more rapidly due to their abbreviated resting phase. If this simple explanation was correct, then telogen-phase LHX2-deficient HF-SCs should display a transcriptional profile analogous to WT HF-SCs, which are activated in early anagen. To test this possibility, we transcriptionally profiled *Lhx2*-cKO and WT HF-SC enriched populations in telogen (Figure S3) and compared their molecular differences to those established for early-anagen-and telogen-phase WT HF-SCs (Lien et al., 2011).

Not surprisingly, some overlap existed between the ≥2× up- or downregulated transcripts in the two groups (Figure 3G). However, more meaningful than these overlaps were the 1,204 mRNAs upregulated by ≥2-fold and the 1,934 mRNAs down-regulated by ≥2-fold when LHX2 was lost in telogen HF-SCs, but not when WT HF-SCs transitioned from

telogen→anagen. These anomalies indicated that there was more to LHX2 deficiency than simply HF-SC overreactivity.

More Than a Third of LHX2-Dependent LHX2 Target Genes Are HF-SC Signature Genes

To gain further insight, we determined the overlap between genes bound by LHX2 (ChIP-seq data) and those differentially expressed ≥2-fold in *Lhx2*-cKO versus WT HF-SCs (microarray data) (Figure 4A). This comparison gave us a shortlist of 323 putative LHX2 target genes whose expression was dependent upon LHX2 (Table S1). As shown by the heat map in Figure 4B, the majority of these genes were downregulated upon loss of LHX2. These results indicated that LHX2 functions primarily as a transactivator of gene expression in HF-SCs.

Interestingly, 36% of the list of LHX2 target genes whose expression was affected ≥2× by LHX2 loss belonged to the signature of genes preferentially expressed in HF-SCs (Lien et al., 2011). This overlap was highly significant, with an overrepresentation factor of 1.8. Moreover, the number of LHX2 targets overlapping this signature was nearly 5× higher when chromatin mapping was performed in HF-SCs (our study) versus embryonic skin (Mardaryev et al., 2011).

To gain further insight into the pathways preferentially regulated by LHX2, we performed Gene Ontology and pathway analyses of the 323 LHX2-bound genes whose expression was altered ≥2-fold by loss of LHX2 (Figure 4C). Wnt-signaling genes were prominent, which was paradoxical given the seemingly operative two-tiered activation of Wnt signaling in the LHX2-deficient SC niche (see Figure 3E). Closer inspection, however, revealed that both positive and negative Wnt pathway regulators were on the list. Most surprisingly, the majority of top categories encompassed proteins involved in the cytoskeleton and in cell-cell and cell-ECM adhesion (Figure 4D).

We selected genes from these three categories to validate our list of LHX2-bound genes that were downregulated in LHX2-deficient bulge cells. Quantitative RT-PCR (qRT-PCR) on independently purified HF-SCs confirmed that putative LHX2-bound genes encoding Wnt regulators and adhesion, extra-cellular-matrix, and/or cytoskeleton molecules were indeed downregulated in *Lhx2*-cKO versus Het HF-SCs (Figure 4E). Representative examples of ChIP-seq profiles of genes from these categories are shown in Figure 4F. Their further validation as bona fide LHX2-bound genes was provided by the enrichment obtained from LHX2-ChIP of HF-SCs (LHX2 positive) but not interfollicular epidermal (IFE) cells (LHX2 negative) (Figures S4A and S4B). The ChIP-qPCR was specific to the region where the LHX2 peak was detected, given that analogous tests for neighboring regions showed no enrichment (see Figure S4B).

To determine whether LHX2 has the capacity to directly regulate the genes that it binds, we carried out luciferase reporter gene assays in cultured cells ± an LHX2 expression vector. The drivers for our reporters were 5′ “enhancer” elements composed of 330–400 bp fragments encompassing the LHX2 binding site(s) of different candidate genes. Relative to the empty backbone (MOCK), each reporter exhibited enhanced luciferase activity in an LHX2-dependent fashion (Figure 4G).

To address whether LHX2 is sufficient to upregulate its target genes, we engineered an in vivo LHX2-inducible system by generating a lentivirus harboring (1) an *Lhx2* complementary DNA driven by a tetracycline regulatory enhancer (TRE), and (2) a *PGK-H2B-RFP* gene to control for transduction (Figure 4H). We then used in utero lentiviral infections (Beronja et al., 2010) to transduce single-layered epidermis of live E9.5 embryos

carrying an epidermally expressed doxycycline (Doxy)-inducible transactivator (rtTA2S-M2-VP16, rtTA) transgene (Nguyen et al., 2006).

Upon Doxy injection of P19 mice, LHX2 was induced in basal epidermis (Figure 4H). qRT-PCR of mRNAs from purified transduced IFE cells ($RFP^{+}\alpha6^{hi}CD34^{-}Sca^{+}$) revealed that HF-SC LHX2-target genes that are normally silent in IFE were now ectopically induced (Figures 4H and S4C). Together, these data bolster our conclusions, first, that LHX2 is a direct positive transcriptional regulator of these genes, and second, that LHX2 may contribute to explaining why these genes are expressed in normal bulge HF-SCs but not in IFE cells.

Perturbations in Bulge Architecture and Apicobasal Polarity of *Lhx2*-cKO HF-SCs

Given the prominence of cytoskeletal and cell-adhesion genes that are direct functional targets of LHX2 and the established reliance of asymmetric cell divisions on proper actin dynamics and cell-cell and cell-substratum adhesion (Lechler and Fuchs, 2005; Luxenburg et al., 2011), we probed deeper into the cellular organization of LHX2-deficient HF-SCs within the bulge. Indeed, in contrast to WT HF-SCs, which were spatially aligned within the outer bulge layer and relative to the inner bulge layer, *Lhx2*-cKO HF-SCs were highly disorganized (Figure 5A). Upon reevaluation of earlier stages, we realized that even at P21, such disorganization in bulge architecture was evident (see box area in Figure 2C).

Further perturbations in cellular organization were revealed by (phalloidin) staining for filamentous actin (F-actin) (Figure 5B). In contrast to WT bulges, which displayed robust F-actin in both inner and outer layers, staining was markedly reduced in the *Lhx2*-cKO bulge. This correlated with the myriad of LHX2 target genes encoding actin regulators that were also downregulated (Figure 4D).

To further pursue the potential relationship between LHX2 targets, F-actin, and cellular organization, we examined the loss-of-function consequences of two LHX2-regulated F-actinassociated proteins. Efficient lentiviral-mediated knockdown of *Flnb* and *Palld* mRNAs in primary cultured keratinocytes resulted in marked alterations in their morphology compared to scramble control cultures (Figures S5A and S5B). Moreover, mitotic keratinocytes displayed an uneven cortical distribution of F-actin and phosphoERM proteins and failed to round up, a process essential for adherent cells within an epithelial sheet (Luxenburg et al., 2011). Axial ratio quantifications of mitotic cells confirmed these marked cell-shape abnormalities (Figure S5C). Notably, similar perturbations occur when *Actb*, encoding actin itself, is knocked down in keratinocytes (Luxenburg et al., 2011). These findings suggest that the perturbations in actin, as visualized within the *Lhx2*-cKO HF-SC niche in vivo and as analyzed by knocking down LHX2-regulated actin-associated proteins in vitro, may contribute significantly to the alterations in shape and organization of *Lhx2*-cKO HF-SCs within their native niche.

The cortical actin-ERM network also functions in apicobasal polarity (Hebert et al., 2012). Interestingly, colabeling for pericentrin and β4-integrin revealed severely compromised apicobasal polarity within the LHX2-deficient SC niche (Figure 5C). As judged by quantification of the angle formed by the centrosome relative to the underlying basement membrane, polarity remained almost perpendicular in both the inner and outer bulge layers of WT HFs, whereas it was considerably more randomized in the *Lhx2*-cKO bulge, particularly among HF-SCs (Figure 5C).

Finally, the perturbations in SC polarity extended beyond the alterations seen in F-actin and its regulators. Similarly diminished in *Lhx2*-cKO HF-SCs was the actin-microtubule crosslinking protein MACF/ACF7, which is essential for Wnt-mediated polarization of

stabilized microtubules in HF-SCs (Wu et al., 2011) (Figure 5D). *Macf1* was also a direct target of LHX2 and was diminished by 4.63 in *Lhx2*-cKO HF-SCs (Table S1). These findings further underscore the importance of LHX2 regulators of cytoskeletal dynamics in maintaining HF-SC polarity within the niche.

Physiological Consequences of Architectural Perturbations in the Bulge

We next addressed whether alterations in cellular organization within the bulge might guide us to a molecular mechanism that would explain the progressive hair thinning and/or balding observed in *Lhx2*-cKO mice (Figure 2E). At 3 months, hair coats of *Lhx2*-cKO mice were already sparse (Figure 6A). Whole-mount immunostaining at second telogen revealed that, unexpectedly, almost the totality of *Lhx2*-cKO HFs had only one bulge, and therefore one hair, instead of the two that typically correspond to the completion of the second hair cycle (Figure 6B).

Two explanations could account for this striking result. Either the old bulge and hair are lost during each hair cycle, or the original bulge is continuously utilized, and a new bulge never forms. To distinguish between these possibilities, we dyed the hair of mice during first telogen, and then monitored hair coats during the subsequent hair cycle. By second telogen, *Lhx2*-cKO mice, but not WT mice, had shed their pink hair coat (Figure 6C). Whole-mount analysis confirmed that in first telogen (P21), both WT and *Lhx2*-cKO HFs had the expected single bulge with fluorescently dyed hair shaft (Figure 6C). However, in second telogen (P45), only WT HFs had the expected two bulges—one with a dyed hair from the first hair cycle (P21) and another with an undyed hair, corresponding to the new hair cycle. By contrast, the only bulge present in *Lhx2*-cKO HFs had an undyed hair shaft, indicating that it was the new bulge. Subsequent hair cycles showed that *Lhx2*-cKO HFs always lose the bulge and hair from the previous cycle (Figure S6A).

To understand when and why the old hair is lost, we monitored *Lhx2*-cKO hair cycles by whole-mount immunofluorescence microscopy. Interestingly, even though the inner bulge layer ($K6^+$) still formed at catagen's end, most $K6^+$ cells were lost during the next anagen (Figure 6D). Loss of these cells had dire consequences, because this layer anchors the old hair to the bulge (Hsu et al., 2011). By full anagen, the old hair was lost, and the two bulges had merged.

Notably, we did not see activated-caspase 3 immunoreactivity or other signs of apoptosis in *Lhx2*-cKO bulge cells at this time (Figure S6A). However, ultrastructural analyses revealed a loss not only of $K6^+$ cells but also the HF-SCs that typically separate the two bulge structures (Figure 6E). Additionally, tenascin C, an ECM protein elevated in the WT HF-SC niche and encoded by the LHX2 target gene *Tnc*, was not only transcriptionally dowregulated but also markedly diminished (Figure S6B; Table S1). Also downregulated was the LHX2 target gene *Itgb6*, encoding β6-integrin, a key component of the tenascin C receptor (Table S1). Together with the discontinuities in β4-integrin staining (Figure 5C), these results suggest that interactions between *Lhx2*-null HF-SCs and their substrata were perturbed. The wide-ranging effects of LHX2 loss on HF-SC polarity, cytoskeletal dynamics, and integrin-ECM connections are likely to contribute collectively to the overall instability of the niche architecture and the accompanying loss of the old bulge and its associated club hair.

The outcome of this instability meant that with each new hair cycle, the *Lhx2*-cKO bulge kept returning to its P21 one-bulge state. Given that $K6^+$ anagen-phase bulge cells produce high levels of FGF18 and BMP6 (Hsu et al., 2011), a reduction in HF-SC inhibitory signals suggested an unanticipated explanation for why the resting phase of *Lhx2*-cKO HFs was always 1–2 days. Indeed, FGF18 immunolabeling was markedly decreased in the old *Lhx2*-

null bulge at this time (Figure 6F). Additionally, transcriptional analysis of *Id* genes, bona fide targets of active BMP signaling, revealed their marked downregulation in *Lhx2*-cKO HF-SCs (Figure 6G). Notably, the highest downregulation was in *Id2*, whose promoter was bound by LHX2 (Table S1).

Without LHX2, HF-SCs Exhibit a Reduced Threshold for Differentiating and Making the Right Fate Choice

Thus far, our studies had upended the prior notion that loss of LHX2 might exhaust the SC pool by promoting continual hair cycling. However, histological analyses revealed an additional contributing factor as remarkable as the perturbations in niche architecture. As shown in the hematoxylin and oil red O-stained whole mounts in Figure 7A (see also Figure S7A), the *Lhx2*-cKO bulge showed signs of what appeared to be sebocytes.

To assess whether the sebocytes emanated from HF-SCs themselves or from the inner layer of terminally differentiated bulge cells, we turned to ultrastructural analyses. In all cases examined, only the basal cells, i.e., HF-SCs, of the niche displayed lipid drops in their cytoplasms (Figure 7B). Some HGs also displayed large sebaceous-like cysts. By contrast, sebocyte-like cells were not observed within the inner bulge layer.

To determine whether the tendency for sebocyte differentiation was rooted in developmental or postnatal defects, we mated *Lhx2*$^{fl/fl}$ mice to *Sox9-CreER* × *Rosa26-YFP*$^{fl/fl}$ mice and induced *Lhx2* ablation in telogen-phase SOX9^{+} HF-SCs. As shown in Figure S7B, mice induced in second telogen and monitored to 8 months of age displayed similar hair loss characterized by ectopic SG development within the *Lhx2*-cKO HF bulge.

A final peculiarity of the aging, bald *Lhx2*-cKO mice was that hair cycling still occurred, but the emerging HFs were short, suggestive of a diminishing ORS (Figure 7C). Moreover, AxinLacZ expression revealed that matrix TACs still generated robust Wnt signaling, a key component of their ability to differentiate into hair cells upon sustained contact with DP. AxinLacZ activity was not detected in the *Lhx2*-cKO bulge, which no longer seemed to recognize its normal role at the helm of HF fate.

The conversion of LHX2-deficient HF-SCs to sebocytes was most frequently observed shortly after the start of each new hair cycle. Moreover, it was exacerbated by hair depilation, which accelerates the activation and self-renewal of remaining HF-SCs (Chen et al., 2012; Hsu et al., 2011). Indeed, repetitive depilations not only accelerated eventual hair loss but also the spontaneous and direct conversion of *Lhx2*-cKO HF-SCs into sebocytes (Figure S7C). Altogether, these data provide compelling evidence that the process of fate instability and spontaneous differentiation in LHX2-deficient HF-SCs is linked to selfrenewal, implying that this defect is rooted in asymmetric cell division.

DISCUSSION

LHX2: A Master Transcriptional Activator in HF-SCs

In this study, we show that LHX2 acts as a positive regulator of a significant number of HF-SC signature genes. It also influences genes encoding components of cytoskeletal and adhesion networks, many of which have been demonstrated previously to affect epidermal and/or HF-SC behavior when ablated (Beck et al., 2011; Giangreco et al., 2009; Wu et al., 2011; Xie et al., 2012). Finally when LHX2 is absent, the normal biology of HF-SCs and their niche are severely compromised.

These findings illuminate LHX2 as a key regulator of bulge SCs, and indeed, more than a third of the functional LHX2 target genes we identified here belong to the HF-SC signature,

i.e., genes preferentially elevated in bulge SCs in vivo over epidermal and downstream HF progenitors (Tumbar et al., 2004). These findings add to the increasing body of evidence that it is not possible to extrapolate the functional importance of a master regulator or its relevant target genes by studying a different cell type or stage of differentiation (Mullen et al., 2011; Trompouki et al., 2011). Since its discovery, LHX2 has been coming to the forefront as a transcription factor important in controlling the behavior of progenitor populations. Beyond HFs, LHX2 has been implicated in the development of the eye, forebrain, limb, and hematopoietic, olfactory, and pituitary systems (Chou et al., 2009; Hägglund et al., 2011; Hirota and Mombaerts, 2004; Pinto do O et al., 2002; Porter et al., 1997; Rodriguez-Esteban et al., 1998; Subramanian et al., 2011; Zhao et al., 2010). Given its increasing importance in the SC field, it will be interesting in the future to see the extent to which LHX2 is a master regulator of these progenitor populations, and if so, how its target genes will be tailored to suit specific needs of different adult SCs.

A Functional Role for LHX2 in Adult HF-SCs

Our prior studies on E16 *Lhx2*-null skin provided the first indications that LHX2 may be important for HF morphogenesis and/or maintenance (Rhee et al., 2006). Our current study with conditional targeting revealed that LHX2's role begins with establishing the bulge niche. Early in HF development, when SCs normally organize into a niche and acquire a quiescent state (Nowak et al., 2008), LHX2-deficient HF-SCs already showed signs of deviating from this behavior.

Despite these abnormalities, HFs still executed the telogen→anagen transition, and in fact did so precociously, as previously suggested by Mardaryev et al. (2011) in their study of heterozygous ($Lhx2^{+/-}$) mice. They also cycled through anagen and catagen phases. In early cycles, they did so along a timeline similar to those of their control littermates. However, LHX2-deficient HF-SCs weren't able to fuel the transit-amplifying (TA)-matrix pool, whose small size was originally thought to reflect a defect in this compartment (Törnqvist et al., 2010). Our findings show that in fact, the TA progeny of LHX2-deficient HF-SCs proliferate and differentiate into the hair shaft and the IRS.

A Role for LHX2 in the Polarization and Organization of HF-SCs within the Niche

By identifying and functionally characterizing target genes that are both bound and regulated by LHX2, we realized that a remarkable number belonged to the molecular scaffold responsible for the maintenance of HF-SC adhesion and actin cytoskeletal organization. Moreover, the physiological defects in the organization and polarity of HF-SCs within the bulge niche upon LHX2 loss are dire. Although the complexity of LHX2's targets, which include actin and microtubule regulators and cell-cell and cell-substratum proteins, preclude our linking any single gene to the disorganization, we unveil the LHX2 dependency of these targets and document their physiological relevance as a cohort of encoded proteins whose functional roles in the polarization of epithelial cells and their cytoskeletons are already well established at an individual level.

An Unexpected Molecular Explanation for Precocious Activation of LHX2-Deficient HF-SCs

Normally, once HF-SCs mature, they remain quiescent throughout most of the hair cycle, a feature that probably ensures their lifelong maintenance (Cotsarelis et al., 1990; Tumbar et al., 2004). While corroborating prior findings (Mardaryev et al., 2011; Rhee et al., 2006) that the frequency and timing of the activation process was altered in the absence of LHX2, we uncovered an unanticipated mechanism underlying this phenomenon.

The first postnatal hair cycle began on cue. Very soon there-after, however, the inner bulge cells that anchor the old club hair were lost, merging the two bulges into one and causing the

hair coat to immediately become 50% sparser than normal. Moreover, because this loss occurred during anagen, the telogen *Lhx2*-cKO HF always resembled the single-bulge state of the first postnatal telogen. This produced a chronic youthful 1-2 day resting phase rather than the age-related prolonged resting phase that comes from multibulge niche structures, which have an increased local density of SC-inhibitory factors (Hsu et al., 2011).

LHX2 at the Crossroads of HF-SC Fate Selection

One of the most surprising results of LHX2 loss was the systematic, age-related transformation of the bulge HF-SC niche into an elaborate array of SG-like structures. With each hair cycle, bulge cells making the incorrect decision left their mark as differentiated sebocytes. As remarkably, some cells at the base of the bulge niche still appeared to make the right decision, even after 6 months of LHX2 loss. However, concomitant with the progressive differentiation of other bulge cells into sebocytes, ORS cell production waned with age. With the DP still present, cells committed to matrix cell conversion exhibited signs of Wnt activity and hair-shaft and IRS differentiation. In the end, a grossly shortened HF emanated from the base of a ristra of SGs.

Sebocyte differentiation has also been reported in HFs that overexpress a K14 transgene encoding a dominant-negative Clim protein. Interestingly, Clim2 interacts with LHX2 (Xu et al., 2007), suggesting that LHX2 may act, at least in part, by recruiting Clim2 to enhance transcription of its target genes. How LHX2 and its associates influence the balance within pilosebaceous units remains unclear. We did not identify factors known to influence sebocyte differentiation, such as PPARγ, Blimp1, or c-Myc, among the LHX2 targets. Rather, without LHX2, HF-SCs seemed to randomly choose between matrix and sebocyte fates in a fashion linked to their activation and self-renewal.

Interestingly, TACs that cannot transactivate Lef1/β-cateninregulated genes also differentiate aberrantly into sebocytes (Merrill et al., 2001; Niemann et al., 2002). Although AxinLacZ was still high in the *Lhx2*-cKO matrix, a commonality between our *Lhx2*-cKO bulge and ΔNLef1 TACs is that in each case, self-renewal and alterations in SC signaling accompanied the incorrect choice. In accounting for the instability in fate choice rather than an absolute defect in lineage selection, it is worth noting that both Wnt-enhancing and -inhibitory genes were among the LHX2 targets, suggesting that within the confines of the niche, the pathway could be misregulated rather than fully suppressed. Though outside the scope of the present study, future experiments will help to assess the extent to which this notion may be correct.

It is additionally relevant that LHX2-deficient bulge SCs are diminished in their apicobasal polarity and actin fibers. These features are essential for asymmetric cell division, the process whereby progenitors divide to generate one new progenitor and one committed daughter (Inaba et al., 2010; Knoblich, 2008; Luxenburg et al., 2011; Ou et al., 2010). Intriguingly, recent studies in *C. elegans* show that an LHX2 ortholog, TTX-3, functions in directly activating terminal differentiation genes in a cholinergic interneuron, AIY (Bertrand and Hobert, 2009). In that study, a transcriptional cascade involving LHX2/TTX-3 coupled the differentiation program to asymmetric division, such that during the terminal division of the AIY mother, an asymmetric Wnt/β-catenin pathway cooperated with TTX-3 to directly restrict downstream expression to only one of the two daughter cells. In that study, TTX-3/Wnt signaling participated in locking one daughter into the differentiation state. Our findings on the normal terminal divisions of mammalian HF-SCs follow the same paradigm, but in this case LHX2 is diminished in the daughter TAC that displays elevated Wnt/β-catenin.

In closing, our study illuminates LHX2 as an orchestrator not only of the signaling pathways that control SC behavior but also the polarity and organization of SCs so that they can properly execute the cell divisions that balance their maintenance and differentiation. Finally, in highlighting the relevance of both intrinsic and extrinsic factors (the niche) in HF-SC behavior, we also uncover parallels that suggest ancient roots for LHX2 in governing SC biology.

EXPERIMENTAL PROCEDURES

Mice, Labeling Experiments, Doxy Induction, and In Utero Injections

Mouse lines are described in Supplemental Experimental Procedures. For label-retaining experiments, mice were injected intraperitoneally (i.p.) with 50 mg/g BrdU (Sigma-Aldrich) every 12 hr for 3 days, and 0.8 mg/ml BrdU was added to drinking water. For EdU pulse-chase experiments, mice were injected i.p. with 25 μg/g EdU (Invitrogen). CreER was induced by topical application of tamoxifen (Sigma-Aldrich; 20 mg/ml in ethanol). Ultrasound-guided lentiviral injection and related procedures have been described (Beronja et al., 2010). TRE-Lhx2 lentiviral overexpression was induced by i.p injection with Doxy (25 mg/g). UV-reactive hair dye was used according to the manufacturer's directions (Manic Panic). Mice were maintained in the Association for Assessment and Accreditation of Laboratory Animal Care-accredited animal facility of The Rockefeller University (RU), and procedures were performed with Institutional Animal Care and Use Committee-approved protocols.

ChIP-Seq Assay and Analysis

All materials, methods, and sequencing for ChIP-seq have been described (Lien et al., 2011). Independent immunoprecipitations were performed on FACS-sorted populations. For each ChIP-seq run, 3×10^6 to $\geq 10^7$ cells were used. Antibodies used for ChIP-seq were rabbit polyclonal anti-mouse LHX2 (Fuchs laboratory). ChIP-seq reads were aligned to the mouse genome (mm9, build 37) and peaks were called with MACS software (Zhang et al., 2008). The reads falling within peaks were 1%, 0.2%, and 0.3% for the three replicates. Of the final LHX2 peaks, 49%, 60%, and 94% were called as peaks in each of the three replicates, whereas 31% were called in all three ChIP-seq rounds. Although purified HF-SCs were preferred for identifying physiologically relevant LHX2 targets, the lower signal-to-noise ratio necessitated our raising the stringency for identifying bona fide peaks. A peak was included in our final list if it was called for both of the first two replicates or for the third replicate alone. The MEME software suite (Bailey et al., 2009) was applied to the sequences under the LHX2 peaks for finding enriched motifs; the program MEME was used for motif discovery, and MAST was used for motif scanning (p value < 0.0001).

Supplementary Material

Refer to Web version on PubMed Central for supplementary material.

Acknowledgments

We thank S. Dewell for assistance in high-throughput sequencing and analysis (RU Genomics Resource Center); S. Mazel, L. Li, S. Semova, and S. Tadesse for FACS sorting (RU FACS facility); the RU Bioimaging Center for advice on image acquisition; and the MSKCC Genomics Core Facility for RNA and microarray processing. We thank E.F.' laboratory members D. Oristian and A. Aldeguer for assistance in mouse research; E. Heller for advice on image analyses and quantifications; M. Nikolova, J. Racelis, S. Chai, E. Wong, and P. Janki for technical assistance; and W.-H. Lien, C. Luxenburg, M. Kadaja, B. Keyes, and C.P. Lu for valuable discussions. A.R.F. was supported by an EMBO Postdoctoral Fellowship. E.F. is an HHMI Investigator. This work was supported by grants to E.F. (National Institutes of Health NIAMS R01AR31737 and New York State Department of Health NYSTEM/C026427) and to D.Z. (NIH/NIMH R21MH099452).

REFERENCES

Bailey TL, Boden M, Buske FA, Frith M, Grant CE, Clementi L, Ren J, Li WW, Noble WS. MEME SUITE: tools for motif discovery and searching. Nucleic Acids Res. 2009; 37(Web Server issue):W202–W208. [PubMed: 19458158]

Beck B, Driessens G, Goossens S, Youssef KK, Kuchnio A, Caauwe A, Sotiropoulou PA, Loges S, Lapouge G, Candi A, et al. A vascular niche and a VEGF-Nrp1 loop regulate the initiation and stemness of skin tumours. Nature. 2011; 478:399–403. [PubMed: 22012397]

Beronja S, Livshits G, Williams S, Fuchs E. Rapid functional dissection of genetic networks via tissue-specific transduction and RNAi in mouse embryos. Nat. Med. 2010; 16:821–827. [PubMed: 20526348]

Bertrand V, Hobert O. Linking asymmetric cell division to the terminal differentiation program of postmitotic neurons in C. elegans. Dev. Cell. 2009; 16:563–575. [PubMed: 19386265]

Blanpain C, Fuchs E. Epidermal homeostasis: a balancing act of stem cells in the skin. Nat. Rev. Mol. Cell Biol. 2009; 10:207–217. [PubMed: 19209183]

Blanpain C, Lowry WE, Geoghegan A, Polak L, Fuchs E. Self-renewal, multipotency, and the existence of two cell populations within an epithelial stem cell niche. Cell. 2004; 118:635–648. [PubMed: 15339667]

Brownell I, Guevara E, Bai CB, Loomis CA, Joyner AL. Nerve-derived sonic hedgehog defines a niche for hair follicle stem cells capable of becoming epidermal stem cells. Cell Stem Cell. 2011; 8:552–565. [PubMed: 21549329]

Chen T, Heller E, Beronja S, Oshimori N, Stokes N, Fuchs E. An RNA interference screen uncovers a new molecule in stem cell self-renewal and long-term regeneration. Nature. 2012; 485:104–108. [PubMed: 22495305]

Chou SJ, Perez-Garcia CG, Kroll TT, O'Leary DD. Lhx2 specifies regional fate in Emx1 lineage of telencephalic progenitors generating cerebral cortex. Nat. Neurosci. 2009; 12:1381–1389. [PubMed: 19820705]

Cotsarelis G, Sun TT, Lavker RM. Label-retaining cells reside in the bulge area of pilosebaceous unit: implications for follicular stem cells, hair cycle, and skin carcinogenesis. Cell. 1990; 61:1329–1337. [PubMed: 2364430]

DasGupta R, Fuchs E. Multiple roles for activated LEF/TCF transcription complexes during hair follicle development and differentiation. Development. 1999; 126:4557–4568. [PubMed: 10498690]

Festa E, Fretz J, Berry R, Schmidt B, Rodeheffer M, Horowitz M, Horsley V. Adipocyte lineage cells contribute to the skin stem cell niche to drive hair cycling. Cell. 2011; 146:761–771. [PubMed: 21884937]

Giangreco A, Jensen KB, Takai Y, Miyoshi J, Watt FM. Necl2 regulates epidermal adhesion and wound repair. Development. 2009; 136:3505–3514. [PubMed: 19783739]

Greco V, Chen T, Rendl M, Schober M, Pasolli HA, Stokes N, Dela Cruz-Racelis J, Fuchs E. A two-step mechanism for stem cell activation during hair regeneration. Cell Stem Cell. 2009; 4:155–169. [PubMed: 19200804]

Hägglund AC, Dahl L, Carlsson L. Lhx2 is required for patterning and expansion of a distinct progenitor cell population committed to eye development. PLoS ONE. 2011; 6:e23387. [PubMed: 21886788]

Hebert AM, DuBoff B, Casaletto JB, Gladden AB, McClatchey AI. Merlin/ERM proteins establish cortical asymmetry and centrosome position. Genes Dev. 2012; 26:2709–2723. [PubMed: 23249734]

Hirota J, Mombaerts P. The LIM-homeodomain protein Lhx2 is required for complete development of mouse olfactory sensory neurons. Proc. Natl. Acad. Sci. USA. 2004; 101:8751–8755. [PubMed: 15173589]

Horsley V, O'Carroll D, Tooze R, Ohinata Y, Saitou M, Obukhanych T, Nussenzweig M, Tarakhovsky A, Fuchs E. Blimp1 defines a progenitor population that governs cellular input to the sebaceous gland. Cell. 2006; 126:597–609. [PubMed: 16901790]

Hsu YC, Fuchs E. A family business: stem cell progeny join the niche to regulate homeostasis. Nat. Rev. Mol. Cell Biol. 2012; 13:103–114. [PubMed: 22266760]

Hsu YC, Pasolli HA, Fuchs E. Dynamics between stem cells, niche, and progeny in the hair follicle. Cell. 2011; 144:92–105. [PubMed: 21215372]

Inaba M, Yuan H, Salzmann V, Fuller MT, Yamashita YM. E-cadherin is required for centrosome and spindle orientation in Drosophila male germline stem cells. PLoS ONE. 2010; 5:e12473. [PubMed: 20824213]

Ito M, Liu Y, Yang Z, Nguyen J, Liang F, Morris RJ, Cotsarelis G. Stem cells in the hair follicle bulge contribute to wound repair but not to homeostasis of the epidermis. Nat. Med. 2005; 11:1351–1354. [PubMed: 16288281]

Kitajima K, Minehata K, Sakimura K, Nakano T, Hara T. In vitro generation of HSC-like cells from murine ESCs/iPSCs by enforced expression of LIM-homeobox transcription factor Lhx2. Blood. 2011; 117:3748–3758. [PubMed: 21343610]

Knoblich JA. Mechanisms of asymmetric stem cell division. Cell. 2008; 132:583–597. [PubMed: 18295577]

Lechler T, Fuchs E. Asymmetric cell divisions promote stratification and differentiation of mammalian skin. Nature. 2005; 437:275–280. [PubMed: 16094321]

Lien WH, Guo X, Polak L, Lawton LN, Young RA, Zheng D, Fuchs E. Genome-wide maps of histone modifications unwind in vivo chromatin states of the hair follicle lineage. Cell Stem Cell. 2011; 9:219–232. [PubMed: 21885018]

Luxenburg C, Pasolli HA, Williams SE, Fuchs E. Developmental roles for Srf, cortical cytoskeleton and cell shape in epidermal spindle orientation. Nat. Cell Biol. 2011; 13:203–214. [PubMed: 21336301]

Mangale VS, Hirokawa KE, Satyaki PR, Gokulchandran N, Chikbire S, Subramanian L, Shetty AS, Martynoga B, Paul J, Mai MV, et al. Lhx2 selector activity specifies cortical identity and suppresses hippocampal organizer fate. Science. 2008; 319:304–309. [PubMed: 18202285]

Mardaryev AN, Meier N, Poterlowicz K, Sharov AA, Sharova TY, Ahmed MI, Rapisarda V, Lewis C, Fessing MY, Ruenger TM, et al. Lhx2 differentially regulates Sox9, Tcf4 and Lgr5 in hair follicle stem cells to promote epidermal regeneration after injury. Development. 2011; 138:4843–4852. [PubMed: 22028024]

McLean CY, Bristor D, Hiller M, Clarke SL, Schaar BT, Lowe CB, Wenger AM, Bejerano G. GREAT improves functional interpretation of cis-regulatory regions. Nat. Biotechnol. 2010; 28:495–501. [PubMed: 20436461]

Merrill BJ, Gat U, DasGupta R, Fuchs E. Tcf3 and Lef1 regulate lineage differentiation of multipotent stem cells in skin. Genes Dev. 2001; 15:1688–1705. [PubMed: 11445543]

Mullen AC, Orlando DA, Newman JJ, Lovén J, Kumar RM, Bilodeau S, Reddy J, Guenther MG, DeKoter RP, Young RA. Master transcription factors determine cell-type-specific responses to TGF-β signaling. Cell. 2011; 147:565–576. [PubMed: 22036565]

Nguyen H, Rendl M, Fuchs E. Tcf3 governs stem cell features and represses cell fate determination in skin. Cell. 2006; 127:171–183. [PubMed: 17018284]

Niemann C, Owens DM, Hülsken J, Birchmeier W, Watt FM. Expression of DeltaNLef1 in mouse epidermis results in differentiation of hair follicles into squamous epidermal cysts and formation of skin tumours. Development. 2002; 129:95–109. [PubMed: 11782404]

Nowak JA, Polak L, Pasolli HA, Fuchs E. Hair follicle stem cells are specified and function in early skin morphogenesis. Cell Stem Cell. 2008; 3:33–43. [PubMed: 18593557]

Ou G, Stuurman N, D'Ambrosio M, Vale RD. Polarized myosin produces unequal-size daughters during asymmetric cell division. Science. 2010; 330:677–680. [PubMed: 20929735]

Pinto do O P, Richter K, Carlsson L. Hematopoietic progenitor/stem cells immortalized by Lhx2 generate functional hematopoietic cells in vivo. Blood. 2002; 99:3939–3946. [PubMed: 12010792]

Plikus MV, Mayer JA, de la Cruz D, Baker RE, Maini PK, Maxson R, Chuong CM. Cyclic dermal BMP signalling regulates stem cell activation during hair regeneration. Nature. 2008; 451:340–344. [PubMed: 18202659]

Porter FD, Drago J, Xu Y, Cheema SS, Wassif C, Huang SP, Lee E, Grinberg A, Massalas JS, Bodine D, et al. Lhx2, a LIM homeobox gene, is required for eye, forebrain, and definitive erythrocyte development. Development. 1997; 124:2935–2944. [PubMed: 9247336]

Rhee H, Polak L, Fuchs E. Lhx2 maintains stem cell character in hair follicles. Science. 2006; 312:1946–1949. [PubMed: 16809539]

Rodriguez-Esteban C, Schwabe JW, Peña JD, Rincon-Limas DE, Magallón J, Botas J, Izpisúa Belmonte JC. Lhx2, a vertebrate homologue of apterous, regulates vertebrate limb outgrowth. Development. 1998; 125:3925–3934. [PubMed: 9735354]

Subramanian L, Sarkar A, Shetty AS, Muralidharan B, Padmanabhan H, Piper M, Monuki ES, Bach I, Gronostajski RM, Richards LJ, Tole S. Transcription factor Lhx2 is necessary and sufficient to suppress astrogliogenesis and promote neurogenesis in the developing hippocampus. Proc. Natl. Acad. Sci. USA. 2011; 108:E265–E274. [PubMed: 21690374]

Törnqvist G, Sandberg A, Hägglund AC, Carlsson L. Cyclic expression of lhx2 regulates hair formation. PLoS Genet. 2010; 6:e1000904. [PubMed: 20386748]

Trompouki E, Bowman TV, Lawton LN, Fan ZP, Wu DC, DiBiase A, Martin CS, Cech JN, Sessa AK, Leblanc JL, et al. Lineage regulators direct BMP and Wnt pathways to cell-specific programs during differentiation and regeneration. Cell. 2011; 147:577–589. [PubMed: 22036566]

Tumbar T, Guasch G, Greco V, Blanpain C, Lowry WE, Rendl M, Fuchs E. Defining the epithelial stem cell niche in skin. Science. 2004; 303:359–363. [PubMed: 14671312]

Vasioukhin V, Degenstein L, Wise B, Fuchs E. The magical touch: genome targeting in epidermal stem cells induced by tamoxifen application to mouse skin. Proc. Natl. Acad. Sci. USA. 1999; 96:8551–8556. [PubMed: 10411913]

Wu X, Shen QT, Oristian DS, Lu CP, Zheng Q, Wang HW, Fuchs E. Skin stem cells orchestrate directional migration by regulating microtubule-ACF7 connections through GSK3b. Cell. 2011; 144:341–352. [PubMed: 21295697]

Xie Y, McElwee KJ, Owen GR, Häkkinen L, Larjava HS. Integrin β6-deficient mice show enhanced keratinocyte proliferation and retarded hair follicle regression after depilation. J. Invest. Dermatol. 2012; 132:547–555. [PubMed: 22113470]

Xu X, Mannik J, Kudryavtseva E, Lin KK, Flanagan LA, Spencer J, Soto A, Wang N, Lu Z, Yu Z, et al. Co-factors of LIM domains (Clims/Ldb/Nli) regulate corneal homeostasis and maintenance of hair follicle stem cells. Dev. Biol. 2007; 312:484–500. [PubMed: 17991461]

Zhang Y, Liu T, Meyer CA, Eeckhoute J, Johnson DS, Bernstein BE, Nusbaum C, Myers RM, Brown M, Li W, Liu XS. Modelbased analysis of ChIP-Seq (MACS). Genome Biol. 2008; 9:R137. [PubMed: 18798982]

Zhao Y, Mailloux CM, Hermesz E, Palkóvits M, Westphal H. A role of the LIM-homeobox gene Lhx2 in the regulation of pituitary development. Dev. Biol. 2010; 337:313–323. [PubMed: 19900438]

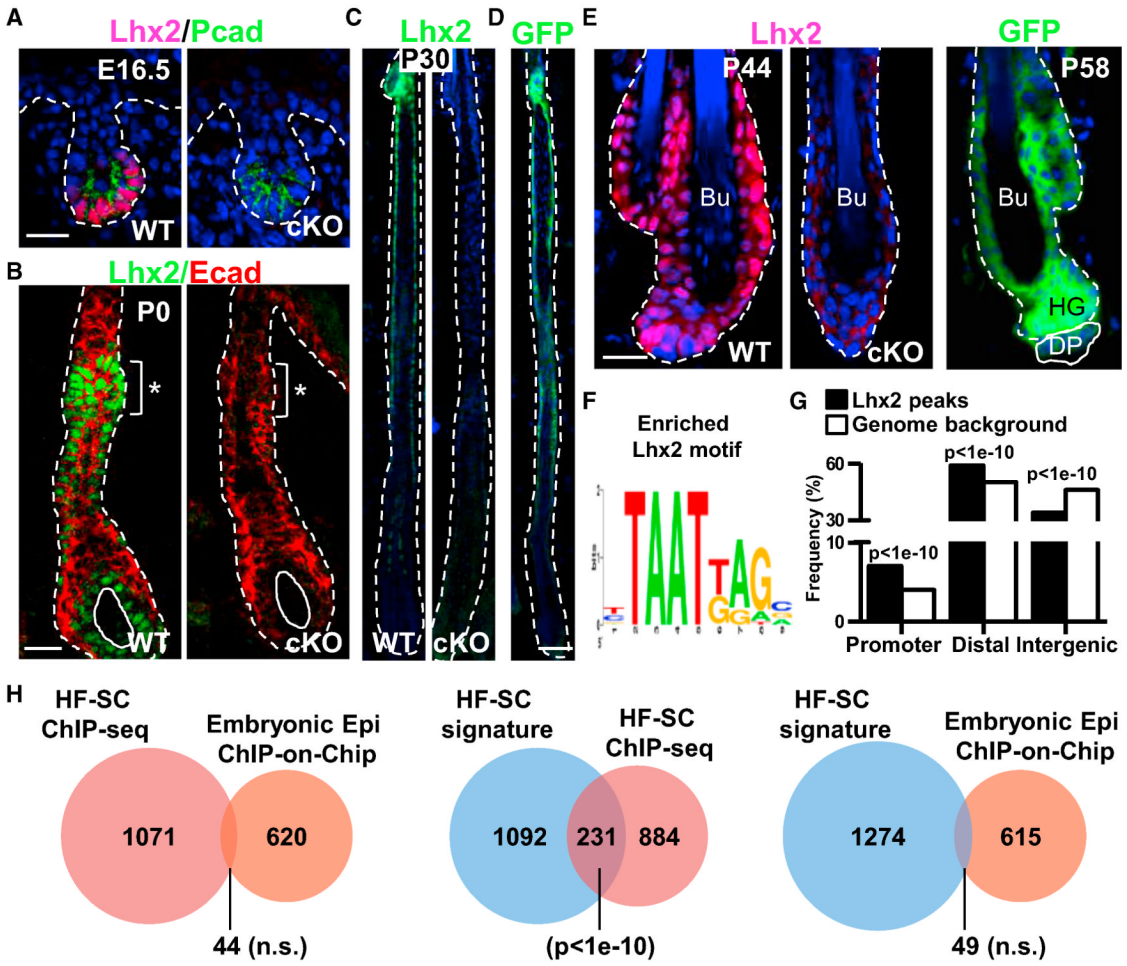

Figure 1. LHX2-Bound Genes in HF-SCs Differ Markedly from Those of Embryonic Skin

(A–E) Antibody specificity and SC-specific expression of LHX2 in adult HFs. LHX2 immunofluorescence of WT and *Lhx2*-cKO backskin sections at E16.5 (A), P0 (B), P30 (C), and second telogen (E); and GFP immunofluorescence of *Lhx2*-EGFP backskin sections at P30 (D) and second telogen (E) stages are shown. Note the correlation between LHX2 immunolabeling and *Lhx2-EGFP* expression and their absence in *Lhx2*-cKO mice. Brackets denote an early bulge (Bu) compartment. Scale bars represent 20 μm (A, B, and E) or 50 μm (C and D). (F) Sequence logo for the most enriched LHX2 motif within LHX2 ChIP-seq peaks. (G) Genomic distribution of LHX2 ChIP-seq peaks compared to background: promoter (±2 kb of transcription start site), distal (from −50 kb to +5 kb of genebodies), and otherwise intergenic peaks. (H) Venn diagrams showing (left) lack of significant overlap of in vivo LHX2-bound targets (ChIP-seq) from HF-SCs versus those of embryonic skin; (middle) significant overlap between HF-SC LHX2-bound targets and HF-SC signature genes; and (right) lack of significant overlap between embryonic-skin LHX2 targets and HF-SC signature genes. White dashed lines denote the epidermal-dermal border; solid lines delineate the DP. The blue channel represents DAPI staining. Epi, Epidermis; n.s., not significant. See also Figure S1.

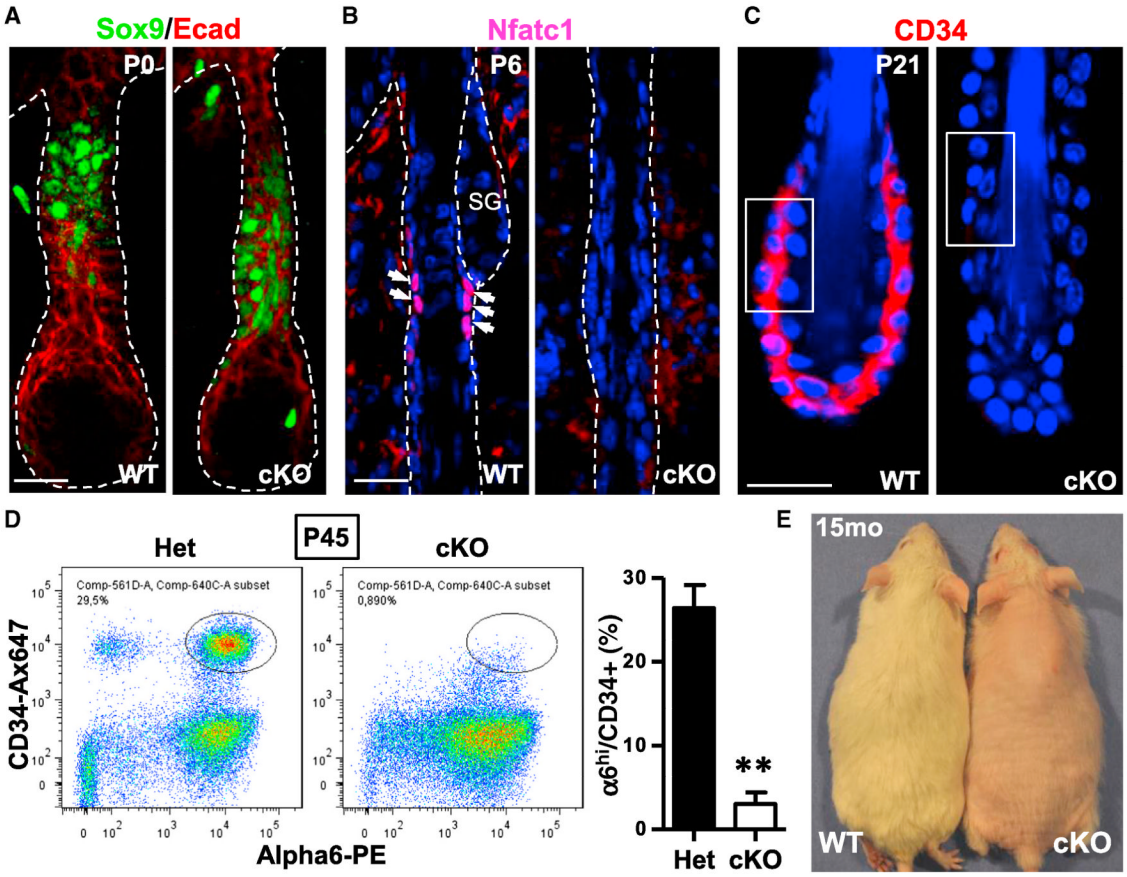

Figure 2. Lhx2-cKO HFs Show Loss of SC Markers and Baldness with Age

(A) Immunofluorescence of P0 backskin shows that the concentration of early bulge cells expressing SOX9 appears lower in the *Lhx2*-cKO HFs. (B) At P6, NFATc1, another early bulge marker, is still undetectable in *Lhx2*-cKO HFs. (C and D) *Lhx2*-cKO HFs lack CD34, a marker of mature HF-SCs acquired after the completion of the first hair cycle by P21. Representative CD34 immunofluorescence (C) and flow-cytometry profiles and their quantification (D) of second telogen HFs (P45) are shown. PE, phycoerythrin; Het, heterozygous. Data are the mean ± SEM. n = 3 mice for each genotype. **p < 0.01. Scale bars represent 20 μm.(E) By 15 months of age (15mo), *Lhx2*-cKO mice are bald. See also Figure S2.

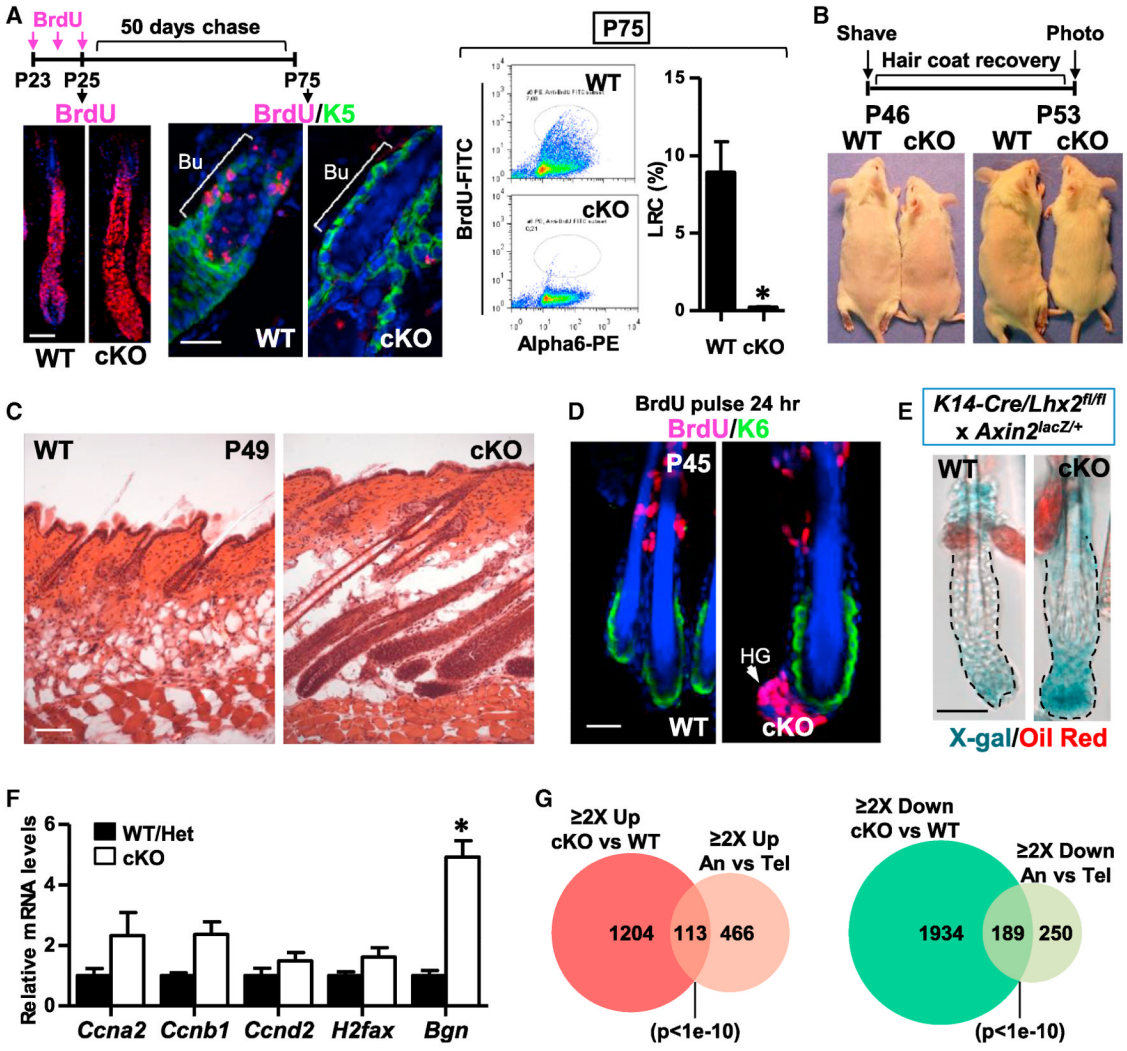

Figure 3. HF-SCs Lacking LHX2 Show Enhanced Activity but Differ Markedly from Normal Anagen-Phase HF-SCs

(A) Lack of label-retaining cells (LRCs) in *Lhx2*-cKO HFs. WT and *Lhx2*-cKO mice were pulsed for 3 days with BrdU in early anagen (P23), followed by 50 days of chase (P75). Representative immunofluorescence illustrates similar BrdU labeling between WT and cKO at P25, but not at P75. Scale bars represent 50 μm (left)and 20 μm (right). Flow-cytometry profiles and quantification of LRCs are shown. FITC, fluorescein isothiocyanate. Data are the mean ± SEM. n = 3 mice for each genotype. *p < 0.05. (B) When shaved at the onset of second telogen (P46), *Lhx2*-cKO hair grows back within one week, in contrast to WT hair. (C) Histological analysis of WT and *Lhx2*-cKO skin at P49. The scale bar represents 100 μm. (D) Representative immunofluorescence of backskin whole mount after a 24 hr BrdU pulse at the onset of WT telogen (P45). Note the HG activation (arrow) in *Lhx2*-cKO HFs. The scale bar represents 20 μm.(E) At the onset of anagen, Wnt signaling ($LacZ^+$ cells) is seen in HFs of both WT and *Lhx2*-cKO $Axin2^{lacZ/+}$ reporter mice. X-gal stainings are of backskin whole mounts. Oil red O staining marks the SGs. The scale bar represents 40 μm. (F) qRT-PCR of HF-SC-enriched populations ($a6^{hi}/YFP^+/ScaI^-/Pcad^-$) of WT/Het and *Lhx2*-cKO mRNAs tested for genes upregulated during a normal telogenanagen transition. Data are the mean ± SEM. n = 5 mice for each genotype. *p < 0.05. (G) Venn diagrams showing the overlap between genes ≥2-fold changed in *Lhx2*-cKO versus WT HF-SCs as

compared to the cohort changed in a normal telogen (Tel)-anagen (An) transition (Lien et al., 2011). See also Figure S3.

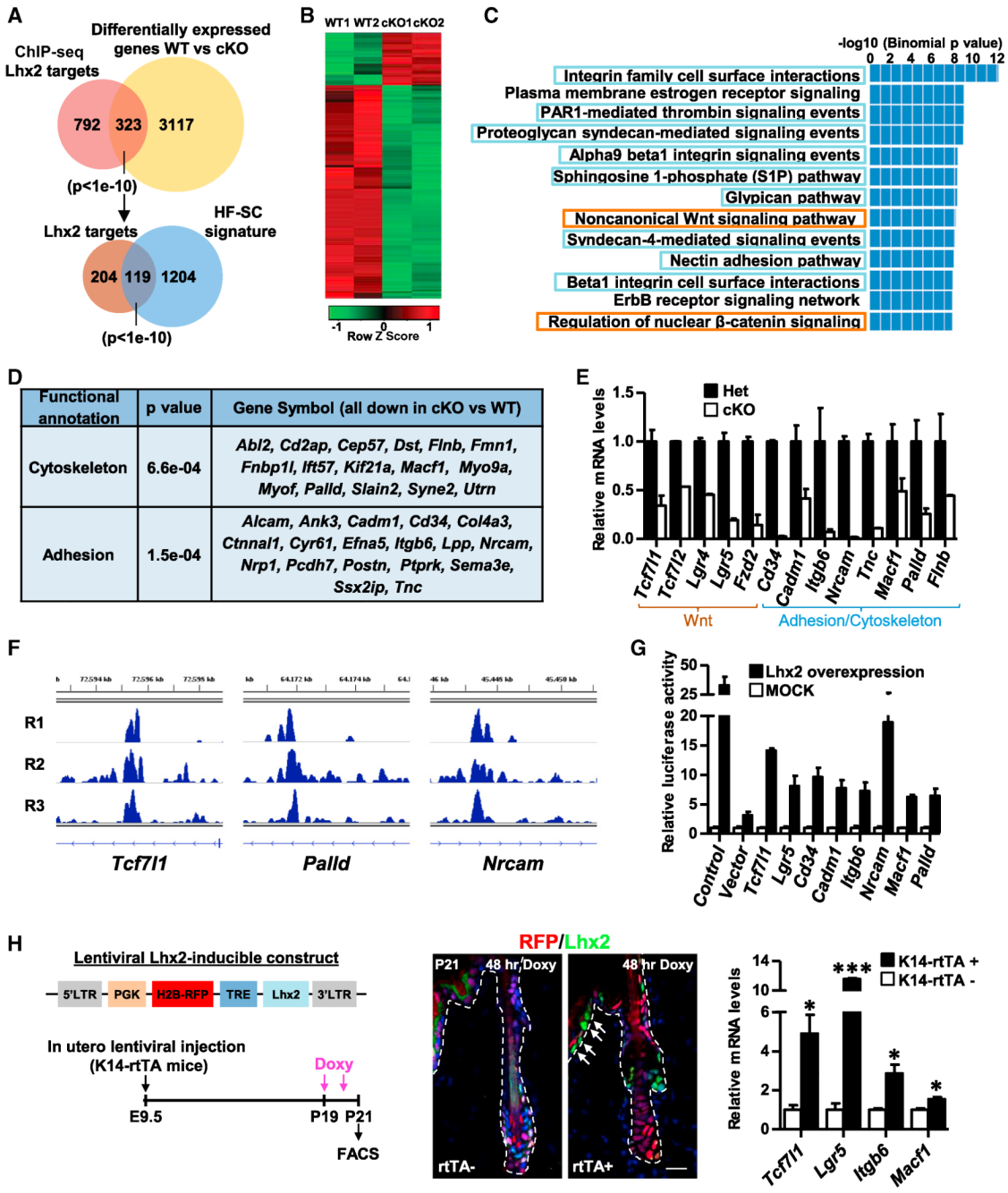

Figure 4. HF-SC ChIP-Seq Analyses of LHX2-Dependent LHX2 Targets Reveal a Preponderance of Genes Encoding Cytoskeletal and Adhesion Proteins

(A) The first Venn diagram shows the overlap of in vivo LHX2-bound targets (ChIP-seq) and mRNAs differentially expressed (microarray analysis) in *Lhx2*-cKO versus WT HF-SCs (FACS-purified from second-telogen HFs). The overlap represents the number of genes bound by LHX2 whose expression is changed ≥2-fold. The second Venn diagram shows the overlap between the 323 LHX2-dependent targets and the HF-SC signature. (B) Heat map of mRNAs differentially expressed between WT and *Lhx2*-cKO HF-SCs. Duplicate data sets are shown. (C) Top biological pathways (as determined by the program GREAT; McLean et al., 2010) that show enrichment among the 323 LHX2-dependent targets in HF-SCs. Note

that cell adhesion/ECM (blue boxes) and Wnt signaling (orange boxes) pathways are among the most significantly enriched. (D) Gene Ontology analyses of these 323 genes highlight “cytoskeleton” and “adhesion” categories. The table shows some examples. (E) qRT-PCR verification of microarray data for a selected group of LHX2-putative target genes. Independent FACS-purified samples were analyzed. Data are the mean ± SEM. n = 2 mice per genotype. (F) LHX2 ChIP-seq profiles of indicated genes. R, replicate. (G) In vitro validation of LHX2 putative targets. Relative luciferase activities driven by sequences (330–400 bp) encompassing LHX2 ChIP-seq peaks. Assays were performed in 293FT cells harboring either an LHX2-expression vector or backbone (MOCK). Our “control” is a luciferase reporter containing five LHX2 binding sites. The “vector” is minimal cytomegalovirus promoter (minCMV)-PGL3. Data are the mean ± SEM. n = 2–5 individual experiments for each construct performed in duplicate wells. (H) In vivo validation of LHX2 putative targets. A schematic of a lentiviral LHX2-inducible construct is shown. PGK-H2B-RFP, marker; TRE, tetracycline (Doxy) regulatory enhancer used to drive *Lhx2* expression. The construct was transduced into skin epithelium by in utero lentiviral infection of E9.5 embryos transgenic for the epidermal-specific, Doxy-sensitive transactivator, rtTA2S-M2-VP16 (rtTA). LHX2 was ectopically induced in the IFE of $rtTA^{+}$ mice at P19, and immunofluorescence was performed at P21. qRT-PCR of FACS-purified IFE cells shows LHX2-dependent activation of LHX2 targets. Data are the mean ± SEM. n = 4 mice per genotype.The scale bar represents 20 μm. See also Figure S4 and Table S1.

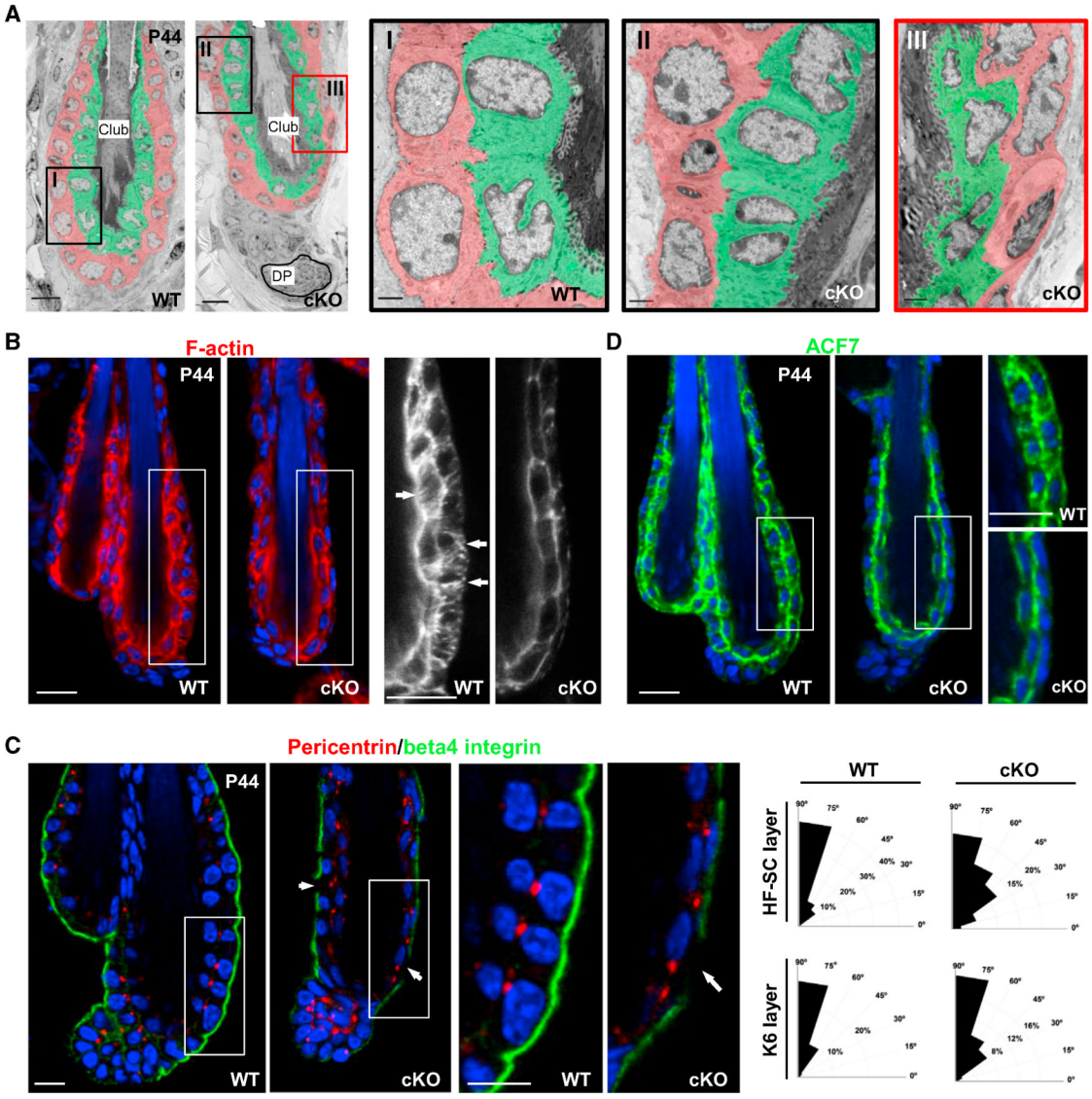

Figure 5. Disruptions in Apicobasal Polarity and Cellular Organization within the *Lhx2*-cKO SC Niche

(A) Ultrastructure analysis of the SC niche of WT and *Lhx2*-cKO HFs at the onset of telogen. The scale bar represents 10 μm. The box areas are magnified in I, II, and III. Note that cells from the outer (HF-SCs, pseudocolored in red) and inner ($K6^+$, pseudocolored in green) layers of the WT bulge are uniformly arranged and cuboidal. By contrast, cellular organization within the cKO bulge appears random. Scale bars represent 2 μm. Club, club hair. (B-D) Whole mount of backskin tissues. (B) Phalloidin staining to mark F-actin fibers (arrows). Boxed areas are magnified at right. Note the paucity of F-actin in the *Lhx2*-cKO bulge. (C) Alterations in apicobasal polarity of *Lhx2*-cKO HF-SCs as assessed by pericentrin localization (normally apical) relative to the basal HF-SC surface (marked by β4-integrin). Note the discontinuities in β4-integrin staining (arrows). Histograms show quantifications of the angles formed by the centrosomal marker (pericentrin) relative to the β4/basement membrane. WT mouse number (n) = 3 (100 basal cells and 65 $K6^+$ cells were analyzed); *Lhx2*-cKO, n = 3 (92 basal cells and 64 $K6^+$ cells were analyzed). (D) The actin-microtubule

crosslinking protein ACF7 (encoded by *Macf1*) is specifically reduced in *Lhx2*-cKO HF-SCs. Scale bars represent 15 μm. See also Figure S5.

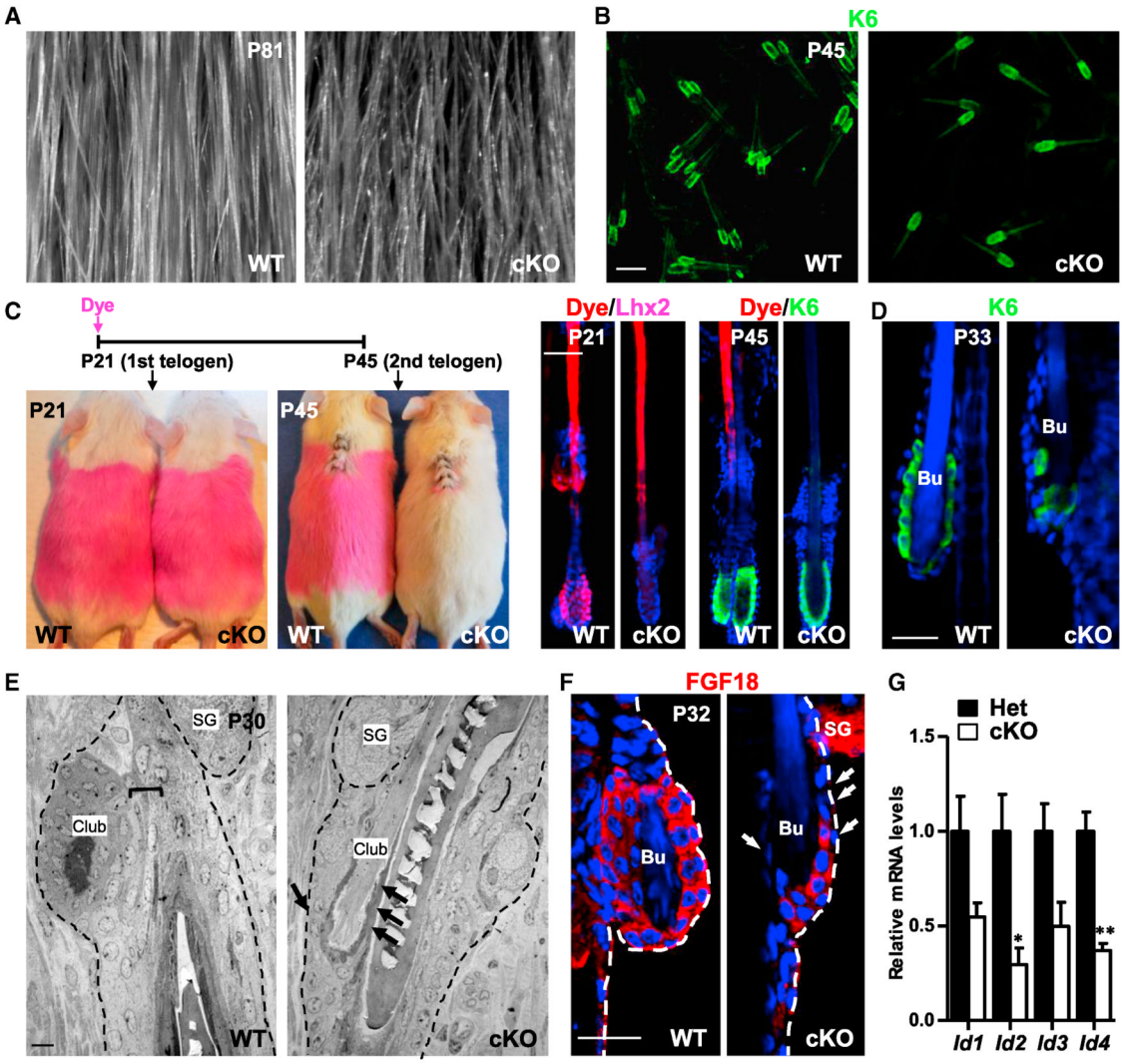

Figure 6.

Lhx2-cKO HFs Lose the Old Bulge and K6$^+$ Inner Bulge Cells during Early Anagen (A) Skin surface showing hair density of WT and *Lhx2*-cKO mice at P81. (B) K6 immunofluorescence of whole-mount backskin HFs at P45. The scale bar represents 100 mm. (C) When hairs from the first cycle were fluorescently dyed at P21 and monitored to the next cycle (P45), *Lhx2*-cKO mice had shed their first hair coat and had only one bulge with undyed (new) hair. The scale bar represents 40 μm.(D) K6 immunofluorescence of whole-mount HFs during anagen. The scale bar represents 20 μm. (E) Ultrastructure analysis of anagen HFs. Brackets indicate the layers of cells that form the boundary between the old bulge and the newly formed HF, which are lost in the *Lhx2*-cKO anagen HFs (arrows). The scale bar represents 10 μm.(F) FGF18 production is reduced in the *Lhx2*-cKO old bulge. Whole-mount backskin HFs are shown. (G) qRT-PCRs of BMP targets in HF-SC-enriched populations of Het and *Lhx2*-cKO mice at the onset of second telogen. Data are the mean ± SEM. Het, n = 4; cKO, n = 3. *p < 0.05; **p < 0.01. See also Figure S6.

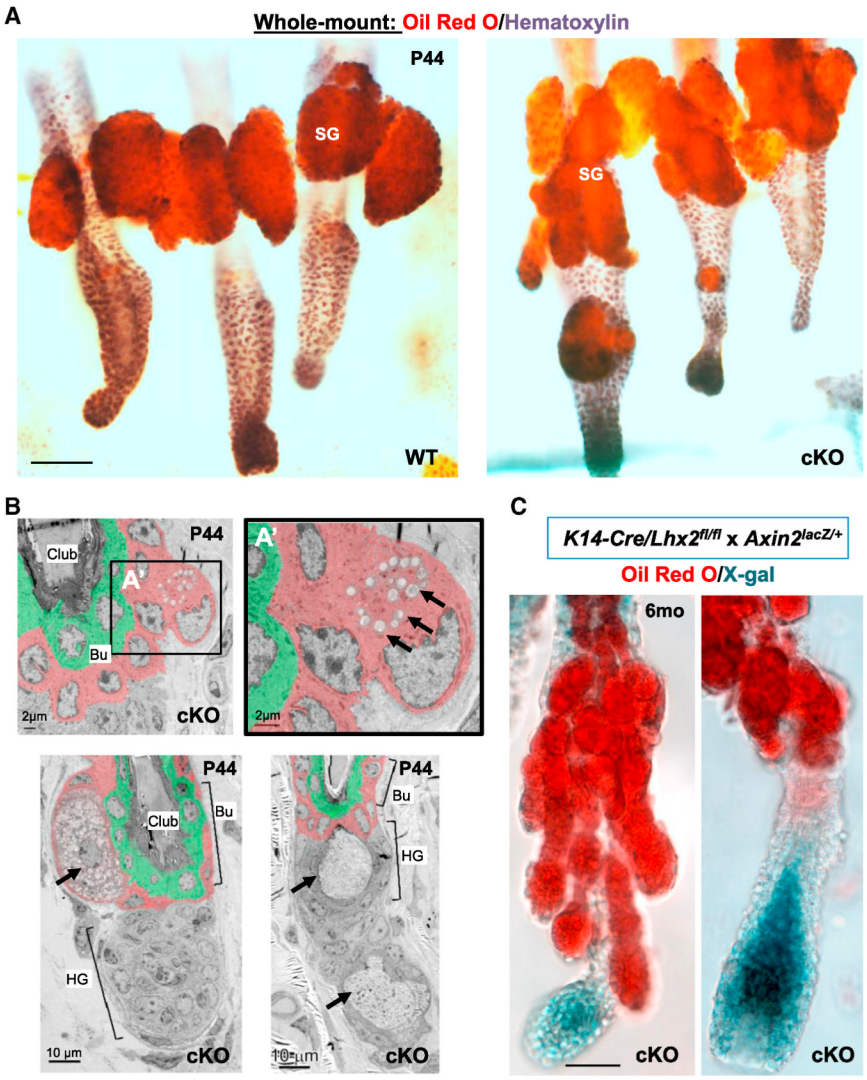

Figure 7.

LHX2-Deficient HF-SCs Spontaneously Differentiate into Sebocytes within Their Niche (A) Oil red O staining of whole-mount tail-skin samples at P44 shows ectopic sebocyte formation in the bulge of tail *Lhx2*-cKO HFs. The scale bar represents 40 μm.(B) Ultrastructure analysis of the *Lhx2*-cKO bulge at P44 shows a developing sebocyte located among HF-SCs (left) never seen in WT. The box area is magnified in A'. Arrows indicate lipid droplets. The scale bar represents 2 μm. Enlarged sebocytes (arrows) within the bulge and HG (right) are shown. The scale bar represents 10 μm.(C) Oil red O staining of 6-month-old *Lhx2*-cKO whole-mount backskin samples in the AxinLacZ background. Samples are counterstained with X-gal. Note that *Lhx2*-cKO HFs still cycle and that TACs are still sensitive to Wnt signaling (right). The scale bar represents 40 μm.See also Figure S7.